Draft version March 22, 2016
Preprint typeset using LaTeX style AASTeX6 v. 1.0

arXiv:1603.06305v1 [astro-ph.SR] 21 Mar 2016

A NON-LTE STUDY OF SILICON ABUNDANCES IN GIANT STARS FROM THE SI I INFRARED LINES IN THE ZJ-BAND[1]

Kefeng Tan and Jianrong Shi
Key Laboratory of Optical Astronomy, National Astronomical Observatories, Chinese Academy of Sciences, Beijing 100012, China

Masahide Takada-Hidai
Liberal Arts Education Center, Tokai University, 4-1-1 Kitakaname, Hiratsuka, Kanagawa 259-1292, Japan

Yoichi Takeda
National Astronomical Observatory of Japan, 2-21-1 Osawa, Mitaka, Tokyo 181-8588, Japan

Gang Zhao
Key Laboratory of Optical Astronomy, National Astronomical Observatories, Chinese Academy of Sciences, Beijing 100012, China

[1]Based on data collected at Subaru Telescope, which is operated by the National Astronomical Observatory of Japan; based on observations made with ESO telescopes at the La Silla Paranal Observatory under programme IDs 266.D-5655(A) and 084.D-0912(A); based on observations carried out at the National Astronomical Observatories (Xinglong, China).

ABSTRACT

We investigate the feasibility of the Si I infrared (IR) lines as Si abundance indicators for giant stars. We find that Si abundances obtained from the Si I IR lines based on the local thermodynamic equilibrium (LTE) analysis show large line-to-line scatter (mean value of 0.13 dex), and are higher than those from the optical lines. However, when the non-LTE effects are taken into account, the line-to-line scatter reduces significantly (mean value of 0.06 dex), and the Si abundances are consistent with those from the optical lines. The typical average non-LTE correction of [Si/Fe] for our sample stars is about −0.35 dex. Our results demonstrate that the Si I IR lines could be reliable abundance indicators provided that the non-LTE effects are properly taken into account.

Keywords: Galaxy: evolution — stars: abundances — stars: atmospheres — stars: late-type

1. INTRODUCTION

Chemical composition of stellar photospheres is a very important tool to investigate the origins of elements as well as the chemical evolution of the galaxies. During the past decades, stellar abundances[1] are mainly determined from optical spectra due to both historical and technical reasons. Though visible light can easily penetrate the atmosphere of the earth, they are subject to the obscuring of interstellar dust and gas. This makes it difficult to utilize the optical spectra to investigate the chemical abundances of stars suffering heavy interstellar extinction, such as stars in the inner Galactic disk and in the Galactic bulge. In this regard, infrared (IR) spectroscopy is more promising as they are much less affected by the interstellar extinction. The ongoing Apache Point Observatory Galactic Evolution Experiment (APOGEE; Majewski et al. 2015) is such an attempt to use high-resolution and high signal-to-noise (S/N) ratio IR spectroscopy to penetrate the dust that obscures significant fractions of the disk and bulge of the Galaxy. Furthermore, IR spectroscopy could even be used to investigate the chemical abundances of stars beyond our Galaxy. Owning to their large luminosities and peak flux in the IR, red supergiant (RSG) stars are ideal tracers of the chemical abundances of the external galaxies out to large distances (Patrick et al. 2015). This has been verified by chemical abundance analysis of

tan@nao.cas.cn

[1] We follow the classical notation $[A/B] = \log(N_A/N_B)_\star - \log(N_A/N_B)_\odot$ in this work.

RSG stars in the Magellanic Clouds (Davies et al. 2015), in NGC 6822 (Patrick et al. 2015), and in the Sculptor Galaxy (Gazak et al. 2015) using the medium-resolution ($R \sim 3000$–8000) spectra in the J-band obtained by X-shooter (Vernet et al. 2011) and K-band Multi-Object Spectrograph (KMOS; Sharples et al. 2013) mounted on the Very Large Telescope. Evans et al. (2011) showed by simulation that, with future instruments, quantitative IR spectroscopy could even be performed for RSG stars to tens of Mpc. Due to the aforementioned advantages, IR spectroscopy will play a more important role in chemical abundance analysis with existing and forthcoming IR instruments (such as Keck/MOSFIRE, VLT/KMOS, TMT/IRMS, E-ELT/EAGLE, etc.).

In addition to the advantages mentioned above, sometimes IR lines could be better abundance indicators than optical lines. This is the case for silicon (Si) in very metal-poor stars. Si is attributed as an α-element, which is made during oxygen and neon burning in massive stars, and later ejected to the interstellar medium by Type II supernovae (SNe) according to Woosley & Weaver (1995). SNe Ia may also produce some Si as suggested by Tsujimoto et al. (1995). Therefore, Si abundances in metal-poor stars could be used to test the SNe and Galactic chemical evolution models. Unfortunately, the optical Si I lines are very weak in very metal-poor stars, so the two strong lines at 3905 and 4102 Å in the near-ultraviolet (NUV) are usually employed to derive Si abundances. However, both of these two lines have defects in abundance determinations. The Si I 3905 Å line is blended by a CH line. Though this CH feature may be weak in dwarf stars with relatively high temperature (Cohen et al. 2004), it could be very strong in cool giant stars (Cayrel et al. 2004). The Si I 4102 Å line falls in the wing of the Hδ line, which makes it not easy to derive accurate Si abundance. In such a situation, the Si I IR lines could be a better alternative to derive Si abundances. There are tens of Si I IR lines that are much stronger than the optical lines and they suffer much less from the problem of blending or continuum normalization compared to the 3905/4102 Å lines. For example, Jönsson et al. (2011) determined Si abundances for ten metal-poor giant stars using three Si I IR lines at 10371, 10844, and 10883 Å. However, their analysis was under the assumption of local thermodynamic equilibrium (LTE) as there was no calculation for the non-LTE effects of the Si I IR lines at that time. Later, Shi et al. (2012) investigated the non-LTE effects of the Si I IR lines in nearby stars (most of which were dwarf stars), and found that the non-LTE effects are important even for metal-rich stars (> 0.1 dex). Bergemann et al. (2013) presented theoretical calculations for the non-LTE effects of four Si I lines in the J-band for RSG stars. Their results show that the non-LTE abundance correction varies smoothly between -0.4 and -0.1 dex for stars with effective temperature between 3400 and 4400 K.

Considering that Shi et al. (2012) concentrated mainly on main-sequence stars, while Bergemann et al. (2013) focused on the theoretical non-LTE effects, we decided to make a practical investigation on the non-LTE effects of 16 Si I IR lines in giant stars based on observational spectra. In particular, the atomic data and model atom of Shi et al. (2012) were calibrated by requiring that consistent Si abundances could be obtained from different Si I IR lines as well as from the optical lines for the sun, and it is necessary to check whether these still hold true for giant stars. In the next section, we briefly describe the observational data used in this work. Section 3 presents our method of non-LTE calculations and the test of its validity for giants. In Section 4, we apply our method to a sample of metal-poor giant stars and compare our results with the theoretical chemical evolution models of Si. In the last section we briefly summarize our results and conclusions.

2. OBSERVATIONAL DATA

The sample analyzed in this work comprises 16 metal-poor giant program stars as shown in Table 1. These stars were originally observed by Takeda & Takada-Hidai (2011, 2012) in 2009 and 2011 for the purpose of determining sulfur (S) abundances using the S I IR triplet lines. The spectra were obtained using the IR Camera and Spectrograph (IRCS; Kobayashi et al. 2000) in combination with the 188-element curvature-based adaptive optics system (AO188) mounted on the Subaru Telescope. With a resolution of about 20,000, the spectra cover a wavelength range of 1.01–1.19 μm, including several Si I lines that are not (severely) blended. For most of the stars, the S/N ratios of the spectra are higher than 100. The spectra were reduced following the standard procedure using the "echelle" package of IRAF[2]. For more details about the observation and data reduction, please refer to Takeda & Takada-Hidai (2011, 2012).

As mentioned in the introduction, one of our aims is to check whether we could obtain consistent Si abundances from the IR and the optical lines in giant stars. Unfortunately, the optical Si I lines are too weak to give very accurate abundances for our sample stars. So we included another two giant stars (Arcturus and HD 83240) as benchmark stars. The optical Si I lines in these two stars are stronger compared to the 16 sample stars,

[2] IRAF is distributed by the National Optical Astronomy Observatories, which are operated by the Association of Universities for Research in Astronomy, Inc., under cooperative agreement with the National Science Foundation.

Table 1. Sample stars and their stellar parameters. From left to right: star ID, effective temperature, surface gravity, metallicity, microturbulent velocity, reference for stellar parameters, adopted uncertainty for effective temperature, surface gravity, metallicity, and microturbulent velocity, references or note about the calculation of the uncertainty of stellar parameters. For stars with multiple independent measurements of stellar parameters in the references, the standard deviations between different studies were adopted as the uncertainties; for the other stars please see the note in the end of the table.

Star	$T_{\rm eff}$ (K)	$\log g$ (cgs)	[Fe/H] (dex)	ξ ($\rm km\,s^{-1}$)	Ref.	σ_t (K)	σ_g (cgs)	σ_m (dex)	σ_v ($\rm km\,s^{-1}$)	Ref./Note
Arcturus	4281	1.72	−0.55	1.5	a	20	0.08	0.07	0.25	a
HD 83240	4682	2.45	−0.02	1.3	b	84	0.27	0.01	0.03	b, l
BD +23°3130	5000	2.20	−2.60	1.4	c	71	0.22	0.14	0.28	⋆
BD −16°251	4825	1.50	−2.91	1.8	d	71	0.01	0.07	0.28	d, i
BD −18°5550	4750	1.40	−3.06	1.8	d	124	0.00	0.04	0.00	d, f
HD 6268	4735	1.61	−2.30	2.1	e	25	0.01	0.45	0.35	e, f
HD 13979	5075	1.90	−2.26	1.3	f	71	0.22	0.14	0.28	⋆
HD 108317	5310	2.77	−2.35	1.9	g	100	0.15	0.09	0.46	c, f, g, h, i
HD 115444	4721	1.74	−2.71	2.0	h	32	0.52	0.12	0.32	e, h, i
HD 121135	4934	1.91	−1.37	1.6	h	6	0.29	0.03	0.28	f, h
HD 126587	4700	1.05	−3.16	1.7	i	18	0.88	0.25	0.11	c, i
HD 166161	5350	2.56	−1.22	2.3	h	100	0.22	0.14	0.18	f, h, i
HD 186478	4730	1.50	−2.42	1.8	i	76	0.08	0.18	0.10	d, f, h, i
HD 195636	5370	2.40	−2.77	1.5	j	71	0.22	0.14	0.28	⋆
HD 204543	4672	1.49	−1.72	2.0	h	16	0.47	0.21	0.00	f, h, i
HD 216143	4525	1.77	−1.92	1.9	e	8	0.51	0.06	0.48	c, e, f, g
HD 221170	4560	1.37	−2.00	1.6	e	74	0.22	0.14	0.52	c, e, f, g, h
HE 1523−0901	4630	1.00	−2.95	2.6	k	71	0.22	0.14	0.28	⋆

References—a: Takeda et al. (2009); b: Mishenina et al. (2006); c: Fulbright (2000); d: Cayrel et al. (2004); e: Saito et al. (2009); f: Burris et al. (2000); g: Takada-Hidai et al. (2005); h: Simmerer et al. (2004); i: Hansen & Primas (2011); j: Carney et al. (2003); k: Frebel et al. (2007); l: Da Silva et al. (2011).

NOTE—⋆ Only single independent measurement of stellar parameters was available in the references; the median value of the errors of the 12 stars with multiple independent measurements of stellar parameters was adopted as the uncertainties.

which permits us to check whether abundances from the optical and the IR lines are in reasonable agreement. Besides, these two stars have archival IR spectra of very high quality, based on which we could obtain very accurate Si abundances to investigate whether different IR lines produce consistent results. For Arcturus, the optical spectra was adopted from the Visible and Near IR Atlas of the Arcturus Spectrum 3727–9300 Å by Hinkle et al. (2000), and the IR spectra was adopted from the IR Atlas of the Arcturus Spectrum, 0.9–5.3 microns by Hinkle et al. (1995). The typical spectral resolution of the optical and IR spectra of Arcturus is 150,000 and 100,000, respectively. For HD 83240, the optical spectra was adopted from the UVES-POP library (Bagnulo et al. 2003), and the IR spectra was adopted from the CRIRES-POP library (Lebzelter et al. 2012). The typical spectral resolution of the optical and the IR spectra of HD 83240 is 80,000 and 96,000, respectively.

3. METHOD OF NON-LTE CALCULATIONS AND VALIDITY TEST

3.1. *Method of non-LTE calculations*

In this work, we used the same method of non-LTE calculations as Shi et al. (2008, 2009, 2011, 2012). Here, we only give a brief description of the method. The key of non-LTE calculations is the atomic model. The Si atomic model adopted here includes 132 terms of Si I, 41 terms of Si II, and the ground state of Si III. In addition to the radiative bound–bound and bound–free transitions, excitation and ionization induced by inelastic collisions with electrons and hydrogen atoms

Table 2. Atomic data of the Si I lines (adopted from Shi et al. 2008) used for abundance determination. From left to right: wavelength, lower and upper level of the transition, excitation potential (EP) of the lower level, oscillator strength, van der Waals damping constant.

Line (Å)	Transition	EP (eV)	$\log gf$	$\log C_6$
5690.43	$4s\,^3P^o_1-5p\,^3P_1$	4.707	−1.73	−30.294
5701.11	$4s\,^3P^o_1-5p\,^3P_0$	4.707	−1.95	−30.294
6142.49	$3p^3\,^3D^o_3-5f\,^3D_3$	5.619	−1.47	−29.869
6145.02	$3p^3\,^3D^o_2-5f\,^3G_3$	5.616	−1.38	−29.869
10288.90	$4s\,^3P^o_0-4p\,^3S_1$	4.920	−1.65	−30.661
10371.30	$4s\,^3P^o_1-4p\,^3S_1$	4.707	−0.85	−30.659
10585.17	$4s\,^3P^o_2-4p\,^3S_1$	4.954	−0.14	−30.659
10603.45	$4s\,^3P^o_1-4p\,^3P_2$	4.707	−0.34	−30.677
10627.66	$4p\,^1P_1-4d\,^3P^o_2$	5.863	−0.39	−30.692
10661.00	$4s\,^3P^o_0-4p\,^3P_1$	4.920	−0.28	−30.687
10689.73	$4p\,^3D_1-4d\,^3F^o_2$	5.954	−0.08	−29.964
10694.27	$4p\,^3D_2-4d\,^3F^o_3$	5.964	0.06	−29.944
10727.43	$4p\,^3D_3-4d\,^3F^o_4$	5.984	0.25	−29.907
10749.40	$4s\,^3P^o_1-4p\,^3P_1$	4.707	−0.20	−30.689
10784.57	$4p\,^3D_2-4d\,^3F^o_2$	5.964	−0.69	−29.965
10786.88	$4s\,^3P^o_1-4p\,^3P_0$	4.707	−0.34	−30.691
10827.10	$4s\,^3P^o_2-4p\,^3P_2$	4.954	0.21	−30.677
10843.87	$4p\,^1P_1-4d\,^1D^o_2$	5.863	−0.08	−30.145
10882.83	$4p\,^3D_3-4d\,^3F^o_3$	5.984	−0.66	−29.945
10979.34	$4s\,^3P^o_2-4p\,^3P_1$	4.954	−0.55	−30.688

were also taken into account. The atomic data of the spectral lines used for Si abundance determination are given in Table 2. The data were adopted from Shi et al. (2008), where the van der Waals damping constants were computed according to the interpolation tables of Anstee & O'Mara (1991, 1995), and the oscillator strengths were derived by requiring the solar Si abundance $\log(N_{\rm Si}/N_{\rm H}) + 12$ to be 7.5. As for the stellar model atmosphere, we used the revised version of the opacity sampling model MAFAGS-OS (Grupp 2004; Grupp et al. 2009), which is under the one-dimensional (1D) and LTE assumption. The coupled radiative transfer and statistical equilibrium equations were solved with a revised version of the DETAIL program (Butler & Giddings 1985). Chemical abundances were derived by spectrum synthesis using the IDL/FORTRAN-based software package Spectrum Investigation Utility (SIU) developed by Dr. J. Reetz. SIU is an advanced software package which could perform spectrum displaying, continuum normalization, radial velocity correlation/correction, spectrum synthesis (in LTE or non-LTE based on the 1D-LTE model atmosphere MAFAGS-OS mentioned above), etc., interactively. All the input parameters, such as abundance for each element, macroturbulence, rotation, and instrument broadening, could be adjusted interactively, and the synthetic spectrum could be displayed on screen in real time. In most cases, the external broadening of line profiles caused by macroturbulence, rotation, and instrument could be approximated using a simple Gaussian function.

3.2. *Validity test for giants with benchmark stars*

The above method of non-LTE calculations has been proved to be applicable for dwarf stars by Shi et al. (2012). In this section we will test whether it is also valid for giant stars.

3.2.1. *Stellar parameters and uncertainties*

For Arcturus, we adopted the stellar parameters ($T_{\rm eff}$ = 4281 K, $\log g$ = 1.72, [Fe/H] = −0.55, ξ = 1.5 km s^{-1}) from Takeda & Takada-Hidai (2011). They were determined by Takeda et al. (2009) in a full spectroscopic way, i.e., $T_{\rm eff}$ from excitation equilibrium of

Fe I, $\log g$ from ionization equilibrium between Fe I and Fe II, [Fe/H] from Fe I, and ξ from abundance-independence of equivalent width (EW). We noticed that Ramírez & Allende Prieto (2011) also investigated the stellar parameters and abundances of Arcturus using high-quality data and methods that minimize model uncertainties. They determined the effective temperature using model atmosphere fits to the observed spectral energy distribution from the blue to the mid-IR, and the surface gravity using the trigonometric parallax. Their stellar parameters ($T_{\rm eff}$ = 4286 ± 30 K, $\log g$ = 1.66 ± 0.05, [Fe/H] = −0.52 ± 0.04, ξ = 1.74 km s^{-1}) are in excellent agreement with those adopted in this work. Recently, Heiter et al. (2015) presented fundamental determinations of $T_{\rm eff}$ and $\log g$ for 34 *Gaia* FGK benchmark stars. Their determinations were based on the angular diameters, bolometric fluxes, distances, and masses, which are independent of spectroscopy and atmospheric models. They gave a $T_{\rm eff}$ of 4286 ± 35 K and a $\log g$ of 1.64 ± 0.09 for Arcturus. And the [Fe/H] of this star was determined to be −0.52 ± 0.08 (after correction for non-LTE effects) in another work (Jofré et al. 2014) in the *Gaia* FGK benchmark stars series. These values agree well with the two sets of stellar parameters mentioned above, and the offsets between different studies are well within the typical uncertainties of stellar parameters ($\Delta T_{\rm eff}$ = 20 K, $\Delta \log g$ = 0.08, Δ[Fe/H] = 0.07, and $\Delta\xi$ = 0.25 km s^{-1}) given by Takeda et al. (2009). Actually, our calculations show that such differences in stellar parameters had a very small effect on the Si abundance (Δ[Si/Fe] ∼ 0.04 dex).

For HD 83240, we adopted the stellar parameters ($T_{\rm eff}$ = 4682 K, $\log g$ = 2.45, [Fe/H] = −0.02, ξ = 1.3 km s^{-1}) from Mishenina et al. (2006). The effective temperature was determined with very high accuracy (σ = 10–15 K) using the line depth ratios of several iron-peak elements (such as Si, Ti, V, Cr, Fe, and Ni). The surface gravity was derived using two methods, i.e., iron ionization equilibrium and wing fitting of the Ca I 6162 Å line, and both methods give the same result. The metallicity was determined from Fe I lines. We note that according to the investigation of Lind et al. (2012), non-LTE effects of Fe I are negligible for cool ($T_{\rm eff}$ < 5000 K) stars with solar metallicity ([Fe/H] ∼ 0), such as HD 83240. The microturbulent velocity was calculated so that iron abundances do not depend on the EWs. Da Silva et al. (2011) gave different stellar parameters for HD 83240 ($T_{\rm eff}$ = 4801 ± 89 K, $\log g$ = 2.83 ± 0.23, [Fe/H] = −0.03 ± 0.08, ξ = 1.26 ± 0.09 km s^{-1}) based on the traditional spectroscopic method, i.e., excitation equilibrium of Fe I and ionization equilibrium between Fe I and Fe II. Their effective temperature is marginally consistent with that of Mishenina et al. (2006) considering the uncertainty, but their surface gravity shows relatively large discrepancy. Nevertheless, the adoption of stellar parameters for HD 83240 does not affect our validity test because difference in Si abundances determined using the above two sets of stellar parameters is only 0.03 dex.

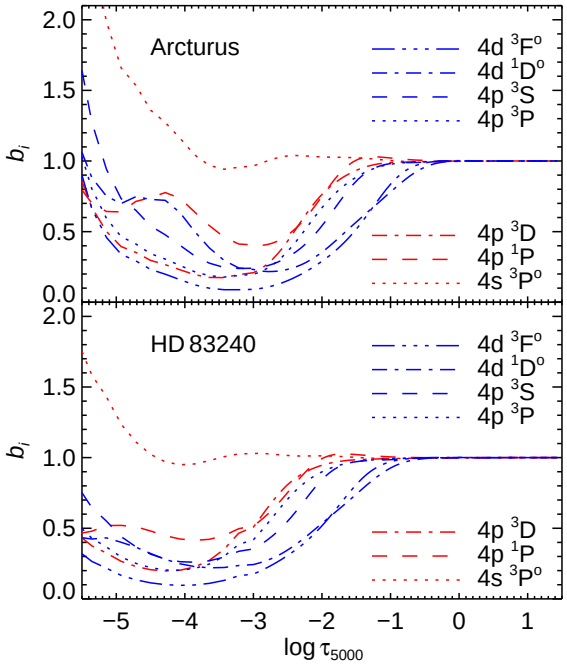

Figure 1. Departure coefficients for the populations of seven selected levels of Si I as a function of continuum optical depth at 5000 Å for Arcturus and HD 83240. The red and the blue lines represent the lower and the upper levels, respectively, of the IR transitions used to determine Si abundances in this work.

3.2.2. *Non-LTE line formation results*

With the stellar parameters we could calculate the level populations in statistical equilibrium. Figure 1 shows the departure coefficients $b_i = n_i^{\rm non\text{-}LTE}/n_i^{\rm LTE}$ for the populations of the seven Si I levels that produce the IR transitions used to determine Si abundances in this work for the two benchmark stars. The red lines represent the lower levels, while the blue lines are the upper levels. It can be seen that, within $\log \tau_{5000} = -3 \ldots -2$, where the Si I IR lines are formed, the departure coefficients of the lower levels (denoted with b_i) are higher than those of the upper levels (denoted with b_j). This means that the line source function S_{ij} is smaller than the local Planck function $B_\nu(T)$ because $S_{ij}/B_\nu(T) \sim b_j/b_i < 1$. As a result, the Si I IR lines are stronger in non-LTE than in LTE, and hence the non-LTE abundance corrections should be negative.

In combination with the calculated populations for the individual levels, Si abundances were then derived by spectrum synthesis of the individual Si I lines. We note here that, due to the enhanced absorption in the line cores in non-LTE, some of the Si I IR lines are so strong

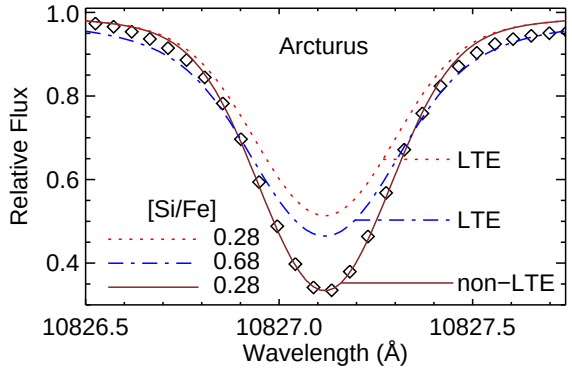

Figure 2. Spectrum synthesis of the Si I 10827 Å line for Arcturus. The diamonds are the observed spectra; the lines are the synthetic spectra in LTE or non-LTE with different [Si/Fe] (see the legend for details).

(EW $\gtrsim$ 150 mÅ) that their observed line profiles could only be reproduced in non-LTE. As an example, Figure 2 shows the spectrum synthesis of the strongest Si I IR line (10827 Å with a EW of 318.3 mÅ) in Arcturus. The solid line shows the best fit to the observed line profile in non-LTE with a [Si/Fe] of 0.28 dex. The dotted line is produced with the same [Si/Fe] but in LTE, which is much weaker in the core of the line. No matter how we adjusted the Si abundance, the observed line profile cannot be reproduced in LTE. In this case, the LTE abundance was derived by simply increasing the [Si/Fe] until the observed EW was reproduced. This led to a [Si/Fe] of 0.68 dex, for which the line profile is shown in dash-dotted line in Figure 2. It can be seen that the core of the line is still much shallower, while the wing is obviously deeper compared to the observed spectra.

Table 3 gives [Si/Fe] determined from the individual optical and IR lines for the two benchmark stars. EWs for the individual lines are also given. As can be seen in Table 3, for both Arcturus and HD 83240, the optical lines are insensitive to the non-LTE effects. This is because these lines are mainly formed in the inner regions of the photospheres ($\log \tau_{5000} > -2$), where the physical conditions are close to LTE. However, as we mentioned above, the regions of line formation for the IR lines are shifted outward to $\log \tau_{5000} = -3 \ldots -2$, where the line source function differs from the local Planck function, and thus the non-LTE effects cannot be neglected. Figure 3 shows the non-LTE correction of [Si/Fe] for the individual Si I IR lines as a function of EW and EP for the two benchmark stars. It can be seen that the non-LTE abundance correction varies between ~ -0.5 dex and ~ -0.05 dex. Though the non-LTE abundance correction seems to be independent of EP, it is correlated with the EW of the line. In general, stronger lines show larger non-LTE effects, while weaker lines show smaller non-LTE effects. Figure 4 shows the [Si/Fe] derived from the individual Si I IR lines as a function of EW and EP

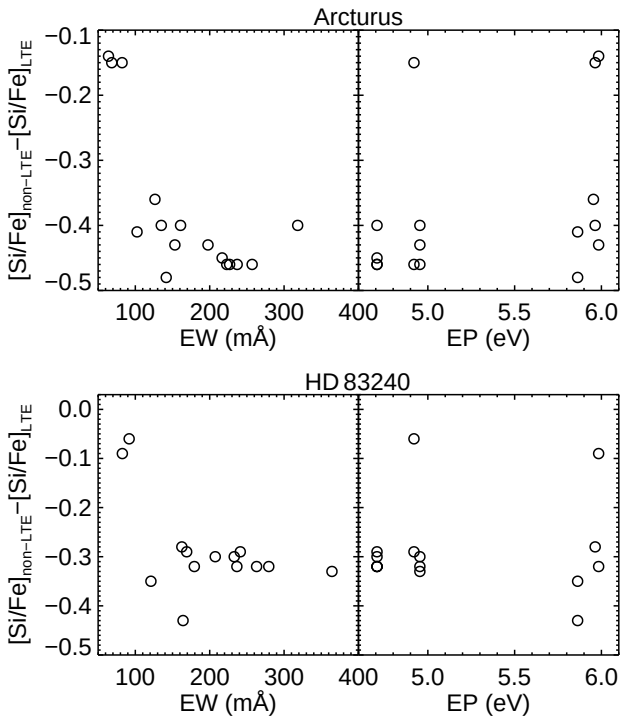

Figure 3. The non-LTE correction of [Si/Fe] for the individual Si I IR lines as a function of EW and EP for Arcturus and HD 83240.

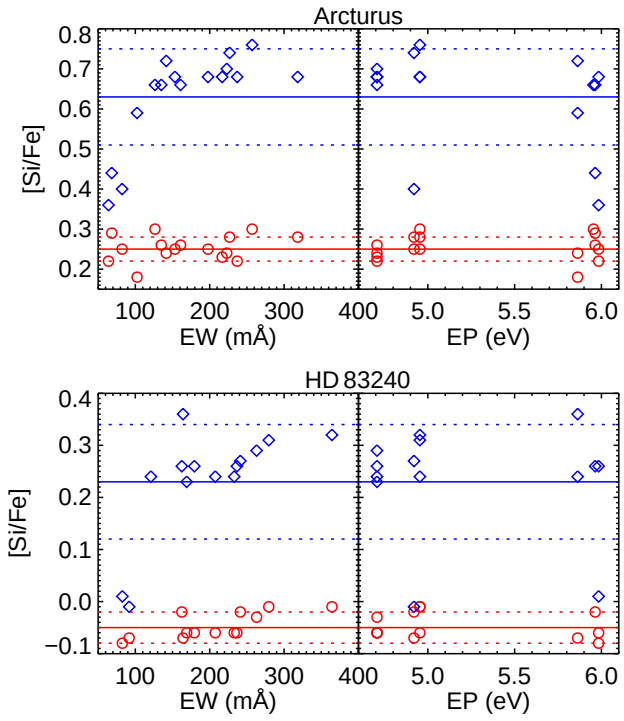

Figure 4. [Si/Fe] from the individual Si I IR lines as a function of EW and EP for Arcturus and HD 83240. The blue and the red are the LTE and the non-LTE results, respectively. The solid lines represent the average values, and the dotted lines indicate the 1σ lower and upper limits for the line-to-line scatter.

Table 3. EWs (in mÅ) and [Si/Fe] for the individual Si I lines of the benchmark stars.

Line	Arcturus			HD 83240		
(Å)	EW	LTE	non-LTE	EW	LTE	non-LTE
5690.43	59.1	0.29	0.29	63.3	−0.09	−0.09
5701.11	48.5	0.31	0.31	54.1	−0.04	−0.04
6142.49	31.2	0.29	0.29	41.4	−0.02	−0.02
6145.05	33.6	0.28	0.28	44.6	−0.02	−0.02
mean		0.29	0.29		−0.04	−0.04
σ		0.01	0.01		0.03	0.03
10288.90	82.3	0.40	0.25	91.8	−0.01	−0.07
10371.30	160.9	0.66	0.26	169.1	0.23	−0.06
10585.17	257.1	0.76	0.30	279.5	0.31	−0.01
10603.45	216.8	0.68	0.23	233.0	0.24	−0.06
10627.66	102.4	0.59	0.18	121.0	0.24	−0.11
10661.00	226.8	0.74	0.28	241.2	0.27	−0.02
10689.73	126.5	0.66	0.30	...	...	...
10694.27	135.0	0.66	0.26	162.6	0.26	−0.02
10727.43	153.3	0.68	0.25	179.4	0.26	−0.06
10749.40	237.0	0.68	0.22	263.1	0.29	−0.03
10784.57	68.4	0.44	0.29	...	...	...
10786.88	223.0	0.70	0.24	236.6	0.26	−0.06
10827.10	318.3	0.68	0.28	364.4	0.32	−0.01
10843.87	141.6	0.72	0.24	164.2	0.36	−0.07
10882.83	64.0	0.36	0.22	82.6	0.01	−0.08
10979.34	197.7	0.68	0.25	207.5	0.24	−0.06
mean		0.63	0.25		0.23	−0.05
σ		0.12	0.03		0.11	0.03

for the two benchmark stars. It is obvious that for both Arcturus and HD 83240, the LTE Si abundances from the IR lines show large line-to-line scatter, but when the non-LTE effects are taken into account, the scatter reduces significantly. Moreover, the average non-LTE Si abundances from the IR lines agree well with those from the optical lines, whereas the LTE results are significantly higher. In a word, our method of non-LTE calculations produces consistent Si abundances from the optical and the IR lines for the two benchmark stars.

We were aware that the two benchmark stars we selected are relatively metal-rich, and it is difficult to justify that our method works also for very metal-poor stars. Unfortunately, in the publicly available archival database, we were not able to find any very metal-poor giant star with high-quality IR spectra in the wavelength range studied in this work. However, in a previous study, Shi et al. (2012) investigated Si abundances for a well-studied very metal-poor giant HD 122563 based on the IR spectra of medium quality ($R \sim 20,000$, S/N $\sim$ 100). The stellar parameters they adopted ($T_{\rm eff} = 4600$ K, $\log g = 1.5$, [Fe/H] $= -2.53$) are in reasonable agreement with the fundamental determinations ($T_{\rm eff} = 4587 \pm 60$ K, $\log g = 1.61 \pm 0.07$, [Fe/H] $= -2.64 \pm 0.22$) of Heiter et al. (2015). The Si abundance determined from the IR spectra ($[{\rm Si/Fe}]_{\rm non\text{-}LTE} = 0.20 \pm 0.01$) agrees well with that from the 3905 and 4102 Å lines ($[{\rm Si/Fe}]_{\rm non\text{-}LTE} = 0.22 \pm 0.05$). Moreover, Jofré et al. (2015) determined Si abundance for HD 122563 using five optical lines[3] by spectrum synthesis. They adopted the stellar parameters from Heiter et al. (2015), and their Si abundance ($[{\rm Si/Fe}]_{\rm non\text{-}LTE} = 0.28 \pm 0.09$) is consistent with those from Shi et al. (2012). Since we used exactly the same method as Shi et al. (2012), it is fair

[3] These lines are very weak; their EWs varies between 1 and 7 mÅ according to Jofré et al. (2015).

to say that our method works also for very metal-poor giant stars.

4. APPLICATION TO METAL-POOR GIANT STARS

In this section, we applied the above method of non-LTE calculations to a sample of 16 metal-poor giant stars.

4.1. *Stellar parameters and uncertainties*

The narrow wavelength range of our IR spectra prevented us from determining stellar parameters for the sample stars by ourselves. So we adopted the stellar parameters from Takeda & Takada-Hidai (2011, 2012), which were taken from nine published studies[4] (see Table 1 for details). Among these studies, different methods have been employed to determine stellar parameters. For example, some studies derive $T_{\rm eff}$ based on spectroscopic method (Fulbright 2000; Simmerer et al. 2004; Hansen & Primas 2011), while the others are based on photometric calibrations; some studies determine $\log g$ using the parallaxes (Simmerer et al. 2004; Takada-Hidai et al. 2005; Saito et al. 2009), while the others utilize the ionization equilibrium between Fe I and Fe II. Therefore, it is not surprising that differences in stellar parameters exist between different studies. Even with the same method, the adoption of different calibrations or line lists by different studies may lead to different results (see the comparison of stellar parameters from different methods for the FGK stars in the *Gaia*-ESO survey by Smiljanic et al. 2014). In the nine studies where we took the stellar parameters, 12 out of 16 sample stars have multiple independent measurements of stellar parameters. We found that, for some stars, the uncertainties of stellar parameters given by the original studies cannot interpret the large differences between different studies. Therefore, for these 12 stars, we took the standard deviations of stellar parameters between different studies as the uncertainties, which are given in columns 7–10 of Table 1. For the rest four stars (BD +23°3130, HD 13979, HD 195636, and HE 1523−0901) with only single measurement of stellar parameters, the median value of the errors of the above 12 stars was adopted.

4.2. *Si abundances and uncertainties*

Si abundances of the sample stars were derived by spectrum synthesis of the individual Si I IR lines. Figure 5 shows the spectrum synthesis of the strong Si I 10585 Å line for two program stars HD 126587 and HD 166161. HD 126587 is the most metal-poor star in our sample, while HD 166161 has the highest effective temperature and surface gravity. It can be seen that, for both of these two stars, the Si I 10585 Å lines are strong enough (EW > 60 mÅ) to be used to determine Si abundances. Table 4 gives [Si/Fe] determined from the individual Si I IR lines for the sample stars. EW for each line is also given.

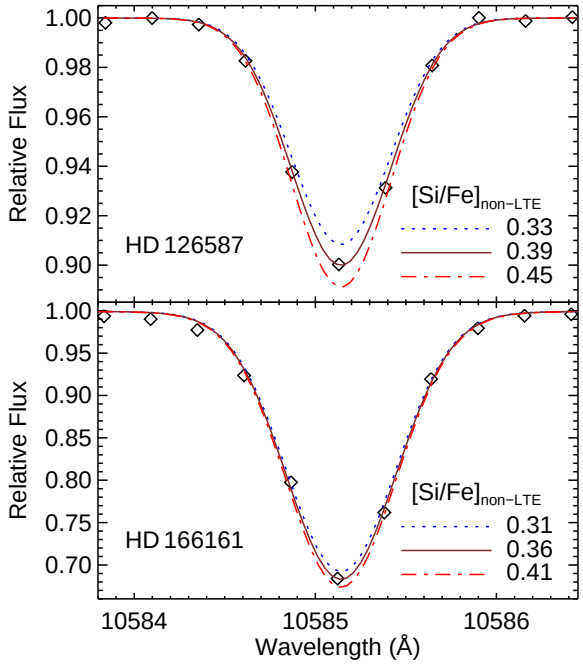

Figure 5. Spectrum synthesis of the Si I 10585 Å line for HD 126587 and HD 166161. The diamonds are the observed spectra; the lines are the synthetic spectra in non-LTE with different [Si/Fe] (see the legend for details).

We were aware that stellar parameters for the sample stars were adopted from different studies, and the effect of inhomogeneous stellar parameters on Si abundances needs to be properly estimated. To do this, for the 12 stars with multiple determinations of stellar parameters, we calculated Si abundances from different stellar parameters, and took the standard deviations as the uncertainties of Si abundances caused by stellar parameters. For the rest four stars with only single measurement of stellar parameters, the median value of the errors (0.12 dex) of the above 12 stars was adopted as the uncertainties caused by stellar parameters. The total errors of [Si/Fe] were then calculated by adding the line-to-line scatters and the errors introduced by stellar parameters in quadrature. Table 5 gives the average [Si/Fe] from the Si I IR lines as well as the associated uncertainties for all the stars investigated in this work.

4.3. *Non-LTE effects of the Si I IR lines*

Figure 6 shows the non-LTE correction of [Si/Fe] for the individual Si I IR lines as a function of EW for the

[4] It is impossible to find independent measurements of stellar parameters for all the sample stars in any single study.

Table 4. EWs (in mÅ) and [Si/Fe] for the individual Si I IR lines of the 16 metal-poor giant stars. For each star, the first row are the EWs; the second and the third row are the LTE and the non-LTE [Si/Fe], respectively.

Star	10371	10585	10603	10627	10661	10689	10694	10727	10749	10784	10786	10827	10843	10979
BD +23°3130	23.1	77.1	54.2	···	54.0	···	···	···	65.7	···	55.0	114.4	···	39.7
	0.38	0.58	0.40	···	0.38	···	···	···	0.41	···	0.40	0.69	···	0.37
	0.16	0.16	0.14	···	0.12	···	···	···	0.11	···	0.13	0.14	···	0.16
BD −16°251	27.5	84.5	57.2	···	60.9	···	···	···	66.7	···	62.0	126.7	···	···
	0.68	0.83	0.63	···	0.66	···	···	···	0.60	···	0.67	1.00	···	···
	0.39	0.35	0.27	···	0.29	···	···	···	0.21	···	0.30	0.29	···	···
BD −18°5550	24.3	79.4	47.9	···	···	···	···	···	70.6	···	49.5	110.9	···	···
	0.72	0.87	0.60	···	···	···	···	···	0.76	···	0.61	0.88	···	···
	0.43	0.41	0.26	···	···	···	···	···	0.34	···	0.26	0.26	···	···
HD 6268	59.7	125.4	86.4	13.8	98.4	26.3	35.1	41.4	107.0	···	89.9	158.8	···	···
	0.50	0.61	0.30	0.26	0.42	0.37	0.41	0.34	0.39	···	0.31	0.57	···	···
	0.27	0.11	0.03	0.21	0.11	0.21	0.24	0.16	0.04	···	0.04	0.00	···	···
HD 13979	···	92.3	57.0	···	64.1	···	23.3	29.5	73.2	···	58.9	120.8	···	43.3
	···	0.57	0.18	···	0.27	···	0.28	0.25	0.28	···	0.19	0.60	···	0.14
	···	0.06	−0.07	···	−0.01	···	0.09	0.04	−0.05	···	−0.07	−0.02	···	−0.04
HD 108317	33.7	99.4	65.7	···	71.7	···	···	41.2	87.1	···	72.9	125.9	···	44.4
	0.49	0.69	0.43	···	0.49	···	···	0.58	0.53	···	0.49	0.60	···	0.33
	0.29	0.26	0.19	···	0.23	···	···	0.39	0.23	···	0.24	0.12	···	0.16
HD 115444	21.7	76.6	46.9	···	54.8	···	···	···	58.3	···	58.7	100.7	···	···
	0.29	0.43	0.21	···	0.30	···	···	···	0.16	···	0.35	0.31	···	···
	0.09	0.08	−0.01	···	0.06	···	···	···	−0.04	···	0.10	−0.09	···	···
HD 121135	115.6	218.9	172.4	70.2	186.1	97.4	114.1	129.6	194.9	34.9	185.8	···	118.0	···
	0.55	1.06	0.76	0.48	0.88	0.62	0.71	0.74	0.83	0.32	0.88	···	0.79	···
	0.21	0.36	0.21	0.23	0.30	0.33	0.36	0.32	0.23	0.24	0.29	···	0.36	···
HD 126587	···	69.1	48.7	···	52.0	···	···	···	53.4	···	48.5	114.3	···	···
	···	0.82	0.70	···	0.73	···	···	···	0.61	···	0.68	1.05	···	···
	···	0.39	0.33	···	0.35	···	···	···	0.23	···	0.31	0.36	···	···
HD 166161	143.9	243.0	204.1	83.2	206.3	111.6	128.9	151.6	221.3	45.6	189.7	288.0	133.2	193.2
	0.76	1.01	0.86	0.54	0.86	0.61	0.68	0.74	0.84	0.44	0.68	0.88	0.74	0.91
	0.40	0.36	0.36	0.36	0.35	0.36	0.37	0.36	0.31	0.36	0.23	0.29	0.41	0.46
HD 186478	48.7	125.2	87.4	···	96.6	···	···	45.4	103.4	···	89.8	159.1	···	···
	0.50	0.82	0.49	···	0.59	···	···	0.55	0.52	···	0.49	0.85	···	···
	0.26	0.25	0.16	···	0.22	···	···	0.33	0.14	···	0.16	0.16	···	···
HD 195636	···	65.4	40.9	···	44.4	···	···	···	···	···	···	···	···	···
	···	0.75	0.54	···	0.58	···	···	···	···	···	···	···	···	···
	···	0.32	0.23	···	0.26	···	···	···	···	···	···	···	···	···
HD 204543	100.3	216.3	165.0	45.5	181.1	66.5	73.4	104.0	173.0	···	157.9	237.7	89.2	···
	0.43	1.09	0.69	0.34	0.86	0.41	0.38	0.58	0.62	···	0.56	0.84	0.58	···
	0.15	0.32	0.16	0.16	0.26	0.21	0.16	0.26	0.06	···	0.08	0.10	0.30	···
HD 216143	64.4	145.5	111.6	···	121.0	···	47.6	61.2	131.9	···	115.4	183.5	40.2	···
	0.17	0.46	0.21	···	0.31	···	0.25	0.27	0.31	···	0.24	0.47	0.14	···
	0.01	0.00	−0.05	···	0.01	···	0.10	0.09	−0.04	···	−0.04	−0.07	0.00	···
HD 221170	83.4	168.9	126.8	31.7	134.9	48.6	57.5	74.1	155.0	···	129.8	201.1	57.1	···
	0.50	0.94	0.58	0.37	0.66	0.44	0.46	0.51	0.78	···	0.58	0.86	0.45	···
	0.23	0.26	0.13	0.22	0.18	0.26	0.25	0.26	0.21	···	0.13	0.16	0.26	···
HE 1523−0901	23.6	83.1	62.9	···	73.1	···	···	···	81.4	···	67.2	127.3	···	···
	0.51	0.62	0.56	···	0.65	···	···	···	0.61	···	0.59	0.68	···	···
	0.26	0.24	0.24	···	0.31	···	···	···	0.24	···	0.26	0.14	···	···

Table 5. Si abundances and uncertainties for all the sample stars. The total errors ($\sigma_{\rm total}$) were calculated by adding the line-to-line scatters ($\sigma_{\rm line}$) and the errors introduced by stellar parameters ($\sigma_{\rm par}$) in quadrature.

Star	[Si/Fe]		$\sigma_{\rm line}$		$\sigma_{\rm par}$	$\sigma_{\rm total}$	
	LTE	non-LTE	LTE	non-LTE		LTE	non-LTE
Arcturus	0.63	0.25	0.12	0.03	0.03	0.12	0.04
HD 83240	0.23	−0.05	0.11	0.03	0.02	0.11	0.04
BD +23°3130	0.45	0.14	0.12	0.02	0.12	0.17	0.12
BD −16°251	0.72	0.30	0.14	0.06	0.01	0.14	0.06
BD −18°5550	0.74	0.33	0.12	0.08	0.06	0.13	0.10
HD 6268	0.41	0.13	0.11	0.09	0.44	0.45	0.45
HD 13979	0.31	−0.01	0.17	0.06	0.12	0.21	0.13
HD 108317	0.51	0.23	0.10	0.08	0.07	0.12	0.11
HD 115444	0.29	0.03	0.09	0.07	0.12	0.15	0.14
HD 121135	0.72	0.29	0.20	0.06	0.05	0.21	0.08
HD 126587	0.77	0.33	0.16	0.06	0.12	0.20	0.13
HD 166161	0.75	0.36	0.15	0.05	0.14	0.21	0.15
HD 186478	0.60	0.21	0.15	0.07	0.16	0.22	0.17
HD 195636	0.62	0.27	0.11	0.05	0.12	0.16	0.13
HD 204543	0.62	0.19	0.22	0.09	0.07	0.23	0.11
HD 216143	0.28	0.00	0.11	0.06	0.11	0.16	0.13
HD 221170	0.59	0.21	0.18	0.05	0.16	0.24	0.17
HE 1523−0901	0.60	0.24	0.06	0.05	0.12	0.13	0.13

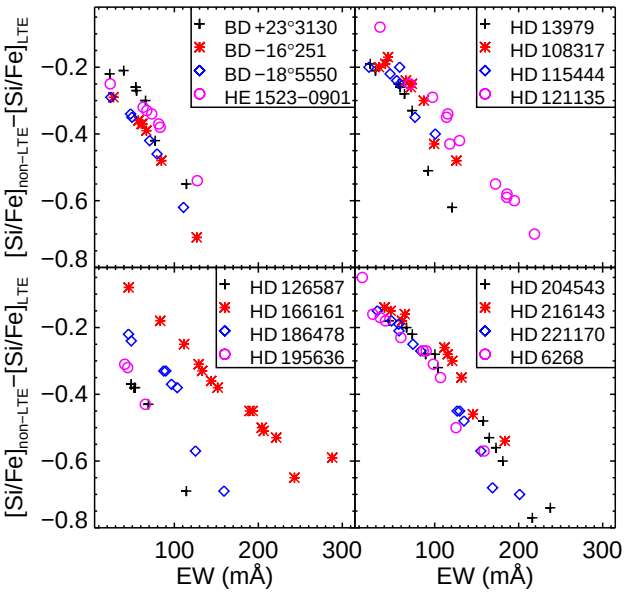

Figure 6. The non-LTE correction of [Si/Fe] for the individual Si I IR lines as a function of EW for the 16 metal-poor giant stars.

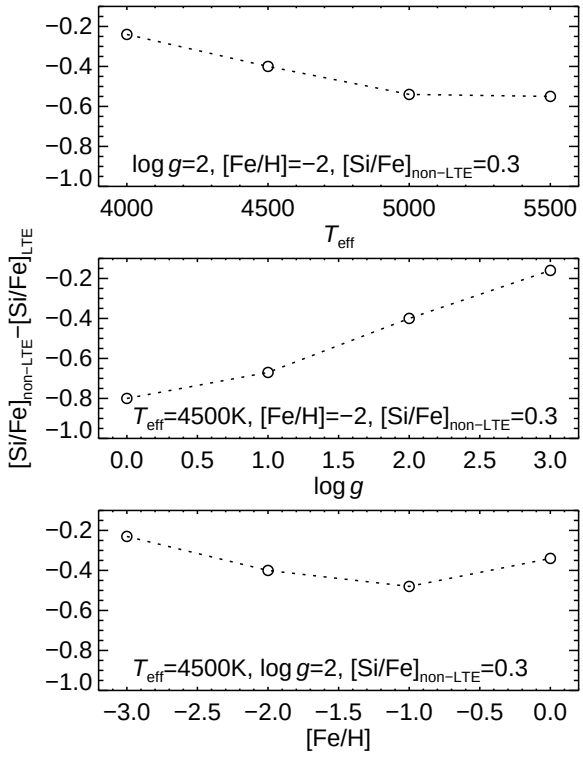

Figure 7. The non-LTE correction of [Si/Fe] for the Si I 10603 Å line as a function of stellar parameters.

sample stars. It can be seen that, the non-LTE effects are significant for all the stars. Besides, the non-LTE abundance corrections differ from line to line; in general, stronger lines show larger non-LTE effects (up to ~ 0.8 dex), while weaker lines show smaller non-LTE effects (as low as ~ 0.1 dex). Overall, the non-LTE abundance corrections show linear correlations with the line strengths for all the stars with similar slopes. But the intercepts of the linear relationships are not necessarily the same; they are dependent on the stellar parameters, especially the surface gravity (see the discussions below). We also explored the dependency of the non-LTE effects on the stellar parameters, and the results are plotted in Figure 7. It can be seen that, the non-LTE abundance corrections are all negative within the range of stellar parameters investigated. Moreover, the non-LTE abundance corrections are more sensitive to surface gravity than effective temperature and metallicity. Stars with lower surface gravity show larger non-LTE effects, while stars with higher gravity show smaller non-LTE effects. Figure 8 shows the line-to-line scatter of [Si/Fe] for the sample stars. It can be seen that, for a given star, the LTE Si abundances show relatively large line-to-line scatter. However, when the non-LTE effects are considered, the scatter reduces significantly, though for some stars they are still relatively large compared to the benchmark stars. This should be partly due to the quality of the spectra (lower resolution and lower S/N compared to the spectra of the benchmark stars) used for abundance determination. Figure 9 shows [Si/Fe] as a function of effective temperature and surface gravity. The results from Shi et al. (2012) which are based on the same IR lines and the same method are also plotted. It can be seen that [Si/Fe] derived from the Si I IR lines based on the non-LTE analysis is independent of $T_{\rm eff}$ and $\log g$.

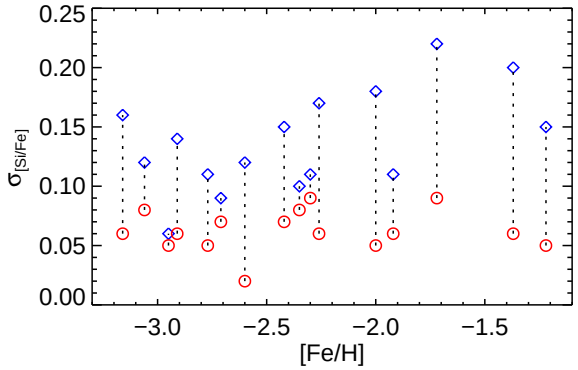

Figure 8. The line-to-line scatter of [Si/Fe] for the 16 metal-poor giant stars. The diamonds and the circles are the LTE and the non-LTE results, respectively.

4.4. *Comparison with other studies*

Shi et al. (2012) investigated the non-LTE effects of the Si I IR lines for 15 nearby stars. Their sample are mostly dwarf stars, and there is only one giant star (HD 122563), for which the average non-LTE correction of [Si/Fe] is −0.26 dex. This is consistent with the results of our sample stars with similar stellar parameters.

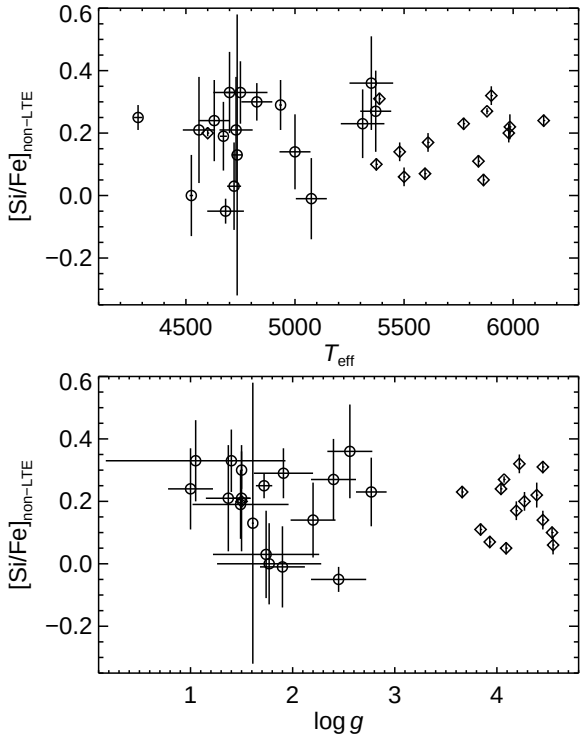

Figure 9. [Si/Fe] derived in non-LTE as a function of effective temperature and surface gravity. The circles are our results; the diamonds are the results from Shi et al. (2012).

Bergemann et al. (2013) calculated the non-LTE effects of four Si I IR lines for RSG stars with effective temperature between 3400 and 4400 K. Unfortunately, we are not able to compare our results directly with those of Bergemann et al. (2013) because the Si I IR lines they investigated are different from those this work. Nevertheless, their results also show negative non-LTE abundance correction, though the magnitude of correction ($-0.4 \ldots -0.1$ dex) is lower than our results. This should be mainly due to that Bergemann et al. (2013) adopted stronger inelastic collisions with neutral hydrogen, which leads to smaller non-LTE effects.

4.5. *Implications for the chemical evolution of Si*

As we mentioned in the introduction, Si abundances could be used to test the SNe and Galactic chemical evolution models. Several previous studies on stellar abundances have investigated the relationship between [Si/Fe] and [Fe/H] (Fulbright 2000; Cayrel et al. 2004; Shi et al. 2009; etc.). While it is generally accepted that [Si/Fe] decreases with [Fe/H] from [Fe/H] ~ -1 to [Fe/H] ~ 0, the behavior of [Si/Fe] below [Fe/H] ~ -1 is still controversial. One reason for this is the significant scatter of [Si/Fe] (ranging from -0.2 to 0.9 dex; see Figure 1 of Shi et al. 2009) below [Fe/H] ~ -1. The dispersion could be due to either the cosmic scatter or the uncertainties in abundance determinations or both. Fulbright (2000) determined Si abundances in LTE for

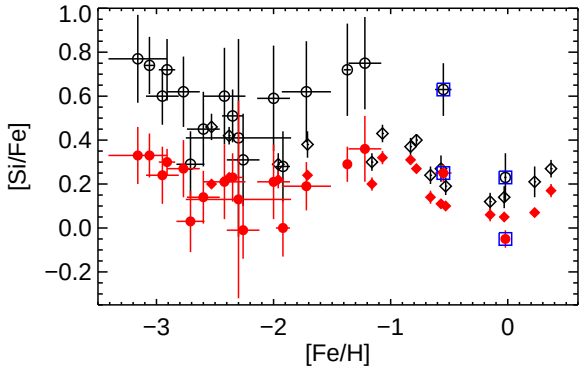

Figure 10. [Si/Fe] as a function of [Fe/H]. Our results are plotted as circles; the results from Shi et al. (2012) are plotted as diamonds. Open and filled symbols correspond to the LTE and the non-LTE abundances, respectively. The results for the two benchmark stars are marked with squares.

168 stars ($-3 <$ [Fe/H] < 0) using 12 Si I lines between 5600 and 7100 Å. Their results showed a decreasing trend of [Si/Fe] with increasing [Fe/H]. Cayrel et al. (2004) performed abundance analysis for 35 very metal-poor stars. Their Si abundances were derived in LTE using the Si I 4102 Å line. The results indicated a slightly increasing trend of [Si/Fe] from [Fe/H] ~ -4 to [Fe/H] ~ -2. Shi et al. (2009, 2011) determined Si abundances in non-LTE for 79 stars based on 11 Si I lines between 3900 and 6300 Å as well as two Si II lines (6347/6371 Å). Their results suggested a flat trend of [Si/Fe] from [Fe/H] ~ -3 to [Fe/H] ~ -1, and then a decreasing trend above [Fe/H] ~ -1. The trend between [Si/Fe] and [Fe/H] derived in this work is shown in Figure 10. The results from Shi et al. (2012) which are obtained using the same IR lines and the same method are also plotted. All the stars in our sample are giants, while most of the stars from Shi et al. (2012) are dwarfs (only one giant). It can be seen that there is no difference in [Si/Fe] between giants and dwarfs in the common metallicity range. As shown in Figure 10, combination of our results with those from Shi et al. (2012) suggests that [Si/Fe] decreases with increasing [Fe/H] in general, though there seems to be a bump around [Fe/H] ~ -1.

There are several Galactic chemical evolution models referring to Si in the literature (Timmes et al. 1995; Samland 1998; Kobayashi et al. 2011; etc.). The chemical evolution calculation of Timmes et al. (1995) predicted that [Si/Fe] increases with [Fe/H] from [Fe/H] ~ -3 to [Fe/H] ~ -2, and then decreases with [Fe/H] until [Fe/H] ~ -0.8. Samland (1998) predicted a constant ratio of [Si/Fe] in the early Galaxy and then a decreasing trend with increasing [Fe/H] due to the contribution of SNe Ia. Kobayashi et al. (2011) presented the evolution of elements (from C to Zn) using chemical evolution models with updated yields of asymptotic giant branch (AGB) stars and core-collapse SNe. Their results

showed that [Si/Fe] gradually decreases with [Fe/H] from [Fe/H] ~ -4 to [Fe/H] ~ -1. Above [Fe/H] ~ -1, [Si/Fe] decreases more rapidly with increasing [Fe/H] due to the contribution of SNe Ia. Interestingly, if the effects of rotating massive stars at $Z = 0$ (in addition to hypernovae, SNe II, SNe Ia, and AGB stars) are taken into account, the [Si/Fe] *versus* [Fe/H] trend that they predicted also shows a small bump around [Fe/H] ~ -1. Such bumps are also predicted for other α-elements, such as S, Ca, and Ti. Therefore, our observational results are most consistent with the predictions of Kobayashi et al. (2011). However, due to the inhomogeneous stellar parameters and small number of sample stars, we are not able to make any conclusive remarks on the Galactic chemical evolution of Si.

5. SUMMARY

As an important α-element, Si is believed to be mainly produced by SNe II, but it is not clear whether SNe Ia also produces some Si. Therefore, Si abundances could be used to test the SNe and Galactic chemical evolution models. Unfortunately, the optical Si I lines are very weak in very metal-poor stars, and the NUV Si I lines are either blended or very difficult to be normalized. In this regard, the Si I IR lines could be better abundance indicators because they are usually much stronger than the optical lines and they suffer much less from the problem of blending or continuum normalization compared to the NUV lines. However, LTE is not a realistic approximation for the line formation of the Si I IR lines, so we have investigated the non-LTE effects of the Si I IR lines in giant stars. The main results could be summarized as follows.

- Si abundances based on the LTE analysis of the Si I IR lines are overestimated (typical value of $\sim$ 0.35 dex for giant stars), and thus are higher than those from the optical lines which are insensitive to the non-LTE effects. However, when our non-LTE calculations are applied, Si abundances from the optical and the IR lines are consistent.

- The non-LTE effects of the Si I infrared lines differ from line to line. In general, stronger lines show larger non-LTE effects (up to $\sim$ 0.8 dex) while weaker lines show smaller non-LTE effects (as low as $\sim$ 0.1 dex). Therefore, it is not surprising that Si abundances based on the LTE analysis of the Si I IR lines show large line-to-line scatter (mean value of 0.13 dex), and when our non-LTE calculations are applied, the scatter reduces significantly (mean value of 0.06 dex).

- The non-LTE effects of the Si I infrared lines are dependent on stellar parameters, among which the surface gravity plays a dominant role. Giant stars show larger non-LTE effects (typical value of $\sim$ 0.35 dex), while dwarf stars show smaller non-LTE effects (typical value of $\sim$ 0.1 dex).

Therefore, the Si I IR lines could be reliable abundance indicators provided that the non-LTE effects are properly taken into account. Our results remind that one should be very careful when using the IR lines to determine chemical abundances under the assumption of LTE. In particular, the APOGEE/APOGEE-2 project will provide high-resolution and high S/N ratio spectra in the H-band for about 400,000 stars, based on which abundances of up to 15 chemical species could be obtained. Investigations of the non-LTE effects for the H-band spectra lines for these elements is of great importance to improving the accuracy of abundance determinations.

We are grateful to the anonymous referee for the valuable suggestions and comments that improve the paper substantially. This work is supported by the National Nature Science Foundation of China under grant Nos. 11103034, 11321064, 11233004, 11390371, 11473033, 11428308, 11273002, U1331120, U1331122, and by the National Basic Research Program of China under grant No. 2014CB845701. This research has made use of the SIMBAD database, operated at CDS, Strasbourg, France, and the NASA's Astrophysics Data System.

REFERENCES

Anstee, S. D., & O'Mara, B. J. 1991, MNRAS, 253, 549
Anstee, S. D., & O'Mara, B. J. 1995, MNRAS, 276, 859
Bagnulo, S., Jehin, E., Ledoux, C., et al. 2003, Msngr, 114, 10
Bergemann, M., Kudritzki, R.-P., Würl, M., et al. 2013, ApJ, 764, 115
Burris, D. L., Pilachowski, C. A., Armandroff, T. E., et al. 2000, ApJ, 544, 302
Butler, K., & Giddings, J. R. 1985, Newsletter on Analysis of Astronomical Spectra No. 9 (London: Univ. London)
Carney, B. W., Latham, D. W., Stefanik, R. P., et al. 2003, AJ, 125, 293
Cayrel, R., Depagne, E., Spite, M., et al. 2004, A&A, 416, 1117
Cohen, J. G., Christlieb, N., McWilliam, A., et al. 2004, ApJ, 612, 1107
Da Silva, R., Milone, A. C., & Reddy, B. E. 2011, A&A, 526, A71
Davies, B., Kudritzki, R.-P., Gazak, Z., et al. 2015, ApJ, 806, 21
Evans, C. J., Davies, B., Kudritzki, R.-P., et al. 2011, A&A, 527, 50
Frebel, A., Christlieb, N., Norris, J. E., et al. 2007, ApJ, 660, 117

Fulbright, J. P. 2000, AJ, 120, 1841
Gazak, J. Z., Kudritzki, R., Evans, C., et al. 2015, ApJ, 805, 182
Grupp, F. 2004, A&A, 420, 289
Grupp, F., Kurucz, R. L., & Tan, K. 2009, A&A, 503, 177
Hansen, C. J., & Primas, F. 2011, A&A, 525, L5
Heiter, U., Jofré, P., Gustafsson, B., et al. 2015, A&A, 582, A49
Hinkle, K., Wallace, L., & Livingston, W. 1995, PASP, 107, 1042
Hinkle, K., Wallace, L., Valenti, J., & Harmer, D. (ed.) 2000, Visible and Near IR Atlas of the Arcturus Spectrum 3727–9300 Å (San Francisco: ASP)
Jofré, P., Heiter, U., Soubiran, C., et al. 2014, A&A, 564, A133
Jofré, P., Heiter, U., Soubiran, C., et al. 2015, A&A, 582, A81
Jönsson, H., Ryde, N., Nissen, P. E., et al. 2011, A&A, 530, A144
Kobayashi, C., Karakas, A. I., & Umeda, H. 2011, MNRAS, 414, 3231
Kobayashi, N., Tokunaga, A. T., Terada, H., et al. 2000, Proc. SPIE, 4008, 1056
Lebzelter, T., Seifahrt, A., Uttenthaler, S., et al. 2012, A&A, 539, A10
Lind, K., Bergemann, M., & Asplund, M. 2012, MNRAS, 427, 50
Majewski, S. R., Schiavon, R. P., Frinchaboy, P. M., et al. 2015, arXiv:1509.05420
Mishenina, T. V., Bienaymé, O., Gorbaneva, T. I., et al. 2006, A&A, 456, 1109
Patrick, L. R., Evans, C. J., Davies, B., et al. 2015, ApJ, 803, 14
Ramírez, I., & Allende Prieto, C. 2011, ApJ, 743, 135
Saito, Y.-J., Takada-Hidai, M., Honda, S., et al. 2009, PASJ, 61, 549
Samland, M. 1998, ApJ, 496, 155
Sharples, R., Bender, R., Agudo Berbel, A., et al. 2013, Msngr, 151, 21
Shi, J. R., Gehren, T., Butler, K., et al. 2008, A&A, 486, 303
Shi, J. R., Gehren, T., Mashonkina, L., et al. 2009, A&A, 503, 533
Shi, J. R., Gehren, T., & Zhao, G. 2011, A&A, 534, A103
Shi, J. R., Takada-Hidai, M., Takeda, Y., et al. 2012, ApJ, 755, 36
Simmerer, J., Sneden, C., Cowan, J. J., et al. 2004, ApJ, 617, 1091
Smiljanic, R., Korn, A. J., Bergemann, M., et al. 2014, A&A, 570, A122
Takada-Hidai, M., Saito, Y., Takeda, Y., et al. 2005, PASJ, 57, 347
Takeda, Y., Kaneko, H., Matsumoto, N., et al. 2009, PASJ, 61, 563
Takeda, Y., & Takada-Hidai, M. 2011, PASJ, 63, S537
Takeda, Y., & Takada-Hidai, M. 2012, PASJ, 64, 42
Timmes, F. X., Woosley, S. E., & Weaver, T. A. 1995, ApJS, 98, 617
Tsujimoto, T., Nomoto, K., Yoshii, Y., et al. 1995, MNRAS, 277, 945
Vernet, J., Dekker, H., D'Odorico, S., et al. 2011, A&A, 536, A105
Woosley, S. E., & Weaver, T. A. 1995, ApJS, 101, 181